

## Symmetry in Mesoscale Circulations Explains Weak Impact of Trade Cumulus Self-Organization on the Radiation Budget in Large-Eddy Simulations

Janssens, M.; Jansson, F.; Alinaghi, P.; Glassmeier, F.; Siebesma, A. P.

**DOI**

[10.1029/2024GL112288](https://doi.org/10.1029/2024GL112288)

**Publication date**

2025

**Document Version**

Final published version

**Published in**

Geophysical Research Letters

**Citation (APA)**

Janssens, M., Jansson, F., Alinaghi, P., Glassmeier, F., & Siebesma, A. P. (2025). Symmetry in Mesoscale Circulations Explains Weak Impact of Trade Cumulus Self-Organization on the Radiation Budget in Large-Eddy Simulations. *Geophysical Research Letters*, 52(3), Article e2024GL112288. <https://doi.org/10.1029/2024GL112288>

**Important note**

To cite this publication, please use the final published version (if applicable). Please check the document version above.

**Copyright**

Other than for strictly personal use, it is not permitted to download, forward or distribute the text or part of it, without the consent of the author(s) and/or copyright holder(s), unless the work is under an open content license such as Creative Commons.

**Takedown policy**

Please contact us and provide details if you believe this document breaches copyrights. We will remove access to the work immediately and investigate your claim.

# Geophysical Research Letters®

## RESEARCH LETTER

10.1029/2024GL112288

### Key Points:

- Simulated shallow cumulus convection spontaneously grows into mesoscale structures across a climatological range of idealized environments
- Letting the convection self-organize gives a systematic  $0.5 \text{ W m}^{-2}$  top-of-atmosphere radiative cooling, due to small offsetting effects
- Mesoscale circulations weakly alter the shortwave cloud-radiative effect because their ascent and descent symmetrically modify cloudiness

### Supporting Information:

Supporting Information may be found in the online version of this article.

### Correspondence to:

M. Janssens,  
[martin.janssens@wur.nl](mailto:martin.janssens@wur.nl)

### Citation:

Janssens, M., Jansson, F., Alinaghi, P., Glassmeier, F., & Siebesma, A. P. (2025). Symmetry in mesoscale circulations explains weak impact of trade cumulus self-organization on the radiation budget in large-eddy simulations. *Geophysical Research Letters*, 52, e2024GL112288. <https://doi.org/10.1029/2024GL112288>

Received 30 AUG 2024

Accepted 17 NOV 2024

© 2025. The Author(s).

This is an open access article under the terms of the [Creative Commons Attribution-NonCommercial-NoDerivs License](#), which permits use and distribution in any medium, provided the original work is properly cited, the use is non-commercial and no modifications or adaptations are made.

## Symmetry in Mesoscale Circulations Explains Weak Impact of Trade Cumulus Self-Organization on the Radiation Budget in Large-Eddy Simulations

M. Janssens<sup>1,2</sup> , F. Jansson<sup>2</sup> , P. Alinaghi<sup>2</sup> , F. Glassmeier<sup>2</sup> , and A. P. Siebesma<sup>2,3</sup>

<sup>1</sup>Wageningen University & Research, Wageningen, The Netherlands, <sup>2</sup>Delft University of Technology, Delft, The Netherlands, <sup>3</sup>Royal Netherlands Meteorological Institute, De Bilt, The Netherlands

**Abstract** We investigate if mesoscale self-organisation of trade cumuli in 150 km-domain large-eddy simulations modifies the top-of-atmosphere radiation budget relative to 10 km-domain simulations, across 77 characteristic, idealized environments. In large domains, self-generated mesoscale circulations produce fewer, larger and deeper clouds, raising the cloud albedo. Yet they also precipitate more than small-domain cumuli, drying and warming the cloud layer, and reducing cloud cover. Consequently, large domains cool slightly less through the shortwave cloud-radiative effect, and slightly more through clear-sky outgoing longwave radiation, for a net cooling ( $-0.5 \text{ W m}^{-2}$ ). This cooling is generally smaller than the large-domain radiation's sensitivity to large-scale meteorological variability, which is similar in small-domain simulations and observations. Hence, mesoscale self-organisation would not alter weak trade-cumulus feedback estimates previously derived from small-domain simulations. We explain this with a symmetry hypothesis: ascending and descending branches of mesoscale circulations symmetrically increase and reduce cloudiness, weakly modifying the mean radiation budget.

**Plain Language Summary** Fields of shallow cumulus clouds over the tropical oceans cool our climate. How much cooling they give with global warming is a long-standing, leading uncertainty in climate projection. Detailed process models estimate this cooling to be resilient to warming-related modifications of the large-scale tropical environment. Yet these models were usually run in small (10 km) domains, while real-world cumuli often grow beyond 100 km in width. Therefore, we compare the cooling in 10 and 150 km-sized detailed process models. Over a large range of idealized environments, the 150 km-domain simulations spontaneously develop large cloud structures, which cannot live in 10 km domains. However, the circulations associated with these large clouds simultaneously reduce cloudiness elsewhere, giving small changes in the overall cloudiness, and cooling. Hence, although they produce cloud patterns more reminiscent of the real world, our large-domain simulations predict a similar resilience to changes in the tropical environment, and thus to warming, as small domains and observations.

## 1. Introduction

Uncertainties in how trade cumuli respond to warming have long shaped the uncertainty margins in climate model estimates of Earth's climate sensitivity (e.g., Bony & Dufresne, 2005; Vial et al., 2013; Zelinka et al., 2020). Significant progress has still been made in constraining the trade-cumulus feedback on warming in recent years, by observing how trade cumuli vary in today's climate at the daily (Vial et al., 2023), seasonal (Brueck et al., 2015) and inter-annual (Cesana et al., 2019; Myers & Norris, 2016; Scott et al., 2020) time scale. By observing which large-scale ( $>500 \text{ km}$ ) "cloud controlling factors" (CCFs, Klein et al., 2017) are responsible for variations in cloudiness in today's world, and combining such sensitivities with estimates of how the CCFs will change with warming, a weak trade-cumulus feedback ( $<0.1 \text{ W m}^{-2} \text{ K}^{-1}$ ) emerges as the most likely outcome (Ceppi & Nowack, 2021; Cesana & Del Genio, 2021; Myers et al., 2021; Sherwood et al., 2020).

Such assessments are complemented by process-understanding from large-eddy simulations (LESs) (Sherwood et al., 2020), traditionally run on small ( $O(10) \text{ km}$ ) domains. These LESs too project a weak trade-cumulus feedback on idealized tropical warming (Blossey et al., 2013; Bretherton, 2015; Bretherton et al., 2013; Radtke et al., 2021; Tan et al., 2017). Yet recent observations highlight that within a 10–500 km ("mesoscale") cloud field, there are large co-variations in cloudiness and vertical motion (George et al., 2021; Vogel et al., 2022), courtesy of mesoscale circulations (George et al., 2023). Equivalently, several LES case studies on

50 km-scale domains and beyond suggest that the convection will “self-organize” into a different regime than in identical small-domain setups (e.g., Alinaghi et al., 2024; Bretherton & Blossey, 2017; Seifert & Heus, 2013; Vogel et al., 2016), through feedbacks between mesoscale circulations and convection. How can observations, which measure the radiation from nature's actual mesoscale cloud patterns, and small-domain LES, which excludes mesoscale self-organisation by definition, then both predict a weak trade cumulus feedback?

To help answer that, we here compare the top-of-atmosphere (TOA) radiation balance between LESs in domains with and without mesoscales. Specifically, we study the Cloud Botany ensemble (Jansson et al., 2023), where we control the initial environment and boundary forcing of square doubly periodic domains of 150 km (henceforth “mesoscale-domain simulations”) and 10 km (“small-domain simulations”) with i. a. five parameters that embody salient CCFs of observational studies: (a) sea surface liquid water potential temperature  $\theta_l$ , varied together with vertically constant  $\theta_l$  offsets throughout the troposphere, (b) near-surface (10 m) geostrophic wind speed ( $U$ ), (c) free-tropospheric lapse rate of  $\theta_l$  ( $\Gamma_{\theta_l}$ ), (d) free tropospheric scale height of total water specific humidity  $q_t$  ( $h_{q_t}$ ), and (e) domain-averaged, cloud-layer subsidence velocity ( $w_{ls}$ ). We vary these CCFs individually and together, giving 103 simulations spanning the climatological envelope of today's trades.

## 2. Self-Organized Mesoscale Cloud Patterns Are Ubiquitous Across Trade-Wind Environments

In the following, we focus on the 77/103 simulations which return cloudy solutions, and run  $\geq 60$  hr. To visualize mesoscale cloud patterns in these simulations, we follow Janssens et al. (2021): For all cloud fields between 6 and 60 hr after initialization at a 5 min interval, we calculate ten “organisation metrics” of the spatial patterning of the clouds. We standardize these metrics over time and simulation, and project the resulting data set onto its principal components (PCs). The two first PCs explain 82% of all 10 metrics' variance across the ensemble. We therefore treat these PCs as effective organisation metrics.

The PCs describe similar pattern characteristics as the satellite images studied by Janssens et al. (2021), though the simulated cloud fields are both smaller (150 vs. 500 km) and forced by a less heterogeneous set of processes. The first PC portrays a typical cloud length scale (Spec. length, Mean cloud object length  $\bar{l}$ ); the second PC captures the complementary length scale of cloud-free regions, measured most closely by the typical “Open sky” area and cloud cover  $f$  (since  $1 - f$  yields the clear sky fraction). Accordingly, we name these components  $L_c$  and  $L_o$ .

Figure 1a) shows examples of cloud fields on the plane spanned by  $L_c$  and  $L_o$ , revealing a broad variety of cloud patterns in the simulations. They include fields of small, uniformly distributed cumuli (left), aggregates of such cumuli in clusters and bands of various sizes (center, center-top), and large, bright clusters and squalls with similarly scaled cloud-free regions, themselves lined by bright clouds (right, similar to e.g. Seifert & Heus, 2013; Vogel et al., 2016; Lamaakel & Matheou, 2022). These large structures also often possess optically thin cloud sheets, resembling the stratiform clouds found atop precipitating shallow convection both in simulations (Dauhut et al., 2023; Vogel et al., 2019) and nature (O et al., 2018; Wood et al., 2018).

Since all simulations are initialized in a spatially homogeneous atmosphere and driven by horizontally homogeneous forcing, all mesoscale cloud patterns are self-organized by feedbacks between convection and mesoscale dynamics. The timeseries in Figures 1c–1e show that every simulation in the ensemble develops such patterns through increasing  $L_c$ , and slightly increasing  $L_o$ . That is, shallow convection spontaneously grows into mesoscale structures across the envelope of environments that is characteristic of the trades.

The growth in  $L_c$  is modulated by an oscillation in both  $L_c$  and  $L_o$  that follows the diurnal cycle of shortwave radiation (Figures 1b–1e). This cycle echoes the diurnal evolution of observed trade cumulus patterns (Vial et al., 2021), and is further explored in Alinaghi et al. (2024). It almost repeats itself after the second simulated day, reflecting how our simulations approach, but do not fully reach, a steady state. We therefore analyze this second day, between 30 and 54 hr.

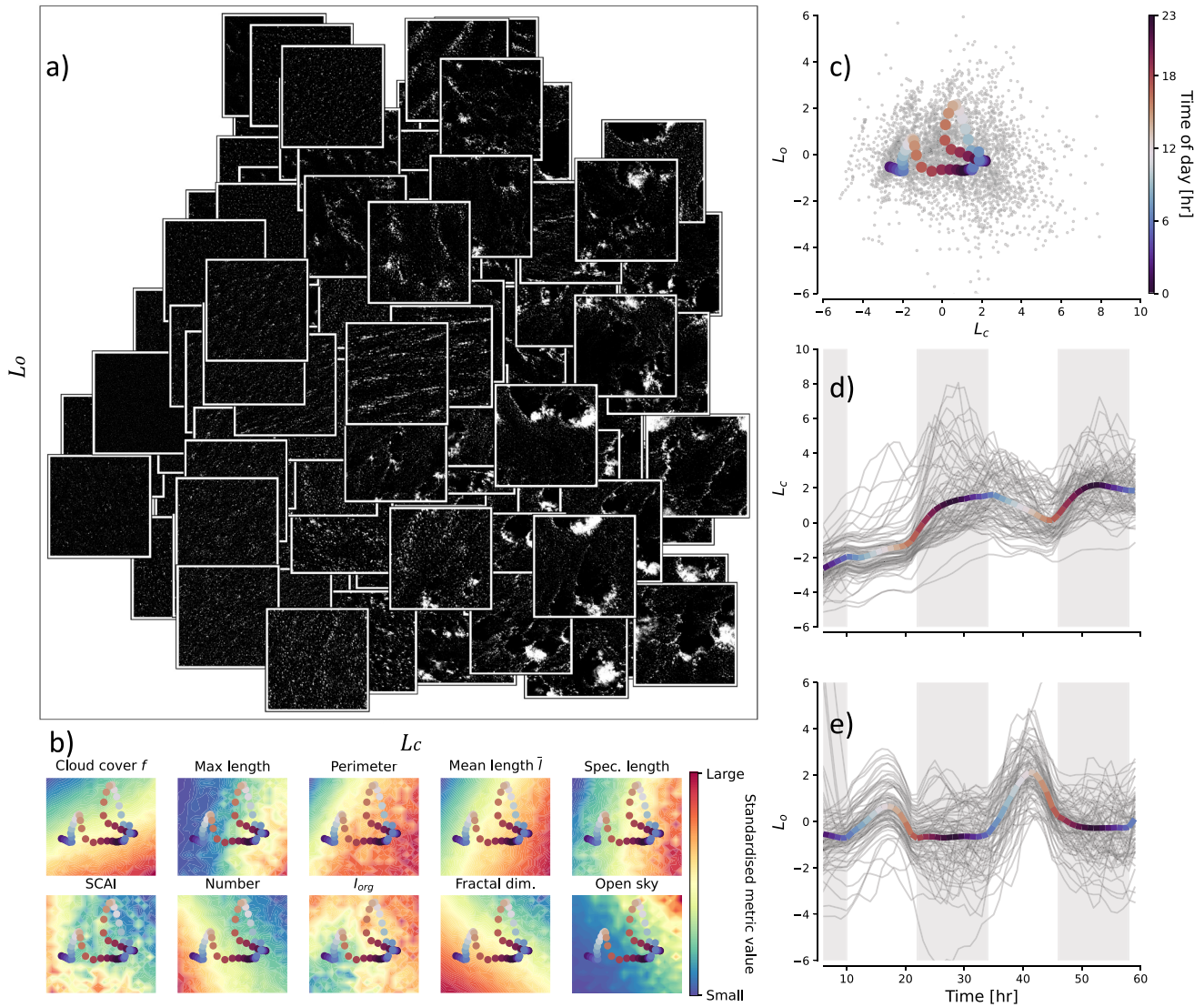


**Figure 1.** (a) Cloud albedo in the plane-parallel approximation by Coakley and Chylek (1975), in example scenes, varying with  $L_c$  and  $L_o$  (b) Excerpts from (a), colored by standardised geometrical organisation metrics, and overlaid by ensemble-mean time evolution, colored by local time of day, see (c). The time-evolution of  $L_c$  (d) and  $L_o$  (e) in all ensemble members is shown between 6 and 60 hr after initialization, also overlaid by the time-of-day-colored ensemble mean. Darkened background shading indicates night.

### 3. Mesoscale Circulations Enhance Rainfall, but Marginally Affect the Top-Of-Atmosphere Radiation Budget

#### 3.1. Rainfall, Cloudiness and Cloud Albedo

To understand how the growth of  $L_c$  and  $L_o$  modifies the TOA radiation balance, we first investigate how it affects the vertical structure of the state variables that ultimately determine the clear- and all-sky radiative transfer:  $\theta_l$ ,  $q_l$ ,  $f$  and cloud-albedo  $\alpha_c$ .

In our mesoscale-domain simulations, the self-organisation primarily affects these quantities by producing an order of magnitude more surface precipitation  $P_s$  ( $0.025 \text{ mm h}^{-1}$ ) than small-domain simulations ( $0.002 \text{ mm h}^{-1}$ ). We believe these differences arise because the mesoscale-domain simulations spontaneously develop mesoscale circulations, which aggregate water vapor into preferentially convecting regions (Bretherton & Blossey, 2017; Janssens et al., 2022; Narenpitak et al., 2021). As a result, substantial mesoscale total water path fluctuations  $I'$  develop: Averaged over  $10 \times 10 \text{ km}^2$  sub-domains, Figure 2a) shows  $I' \sim 2\text{--}4 \text{ mm}$  around the domain-mean

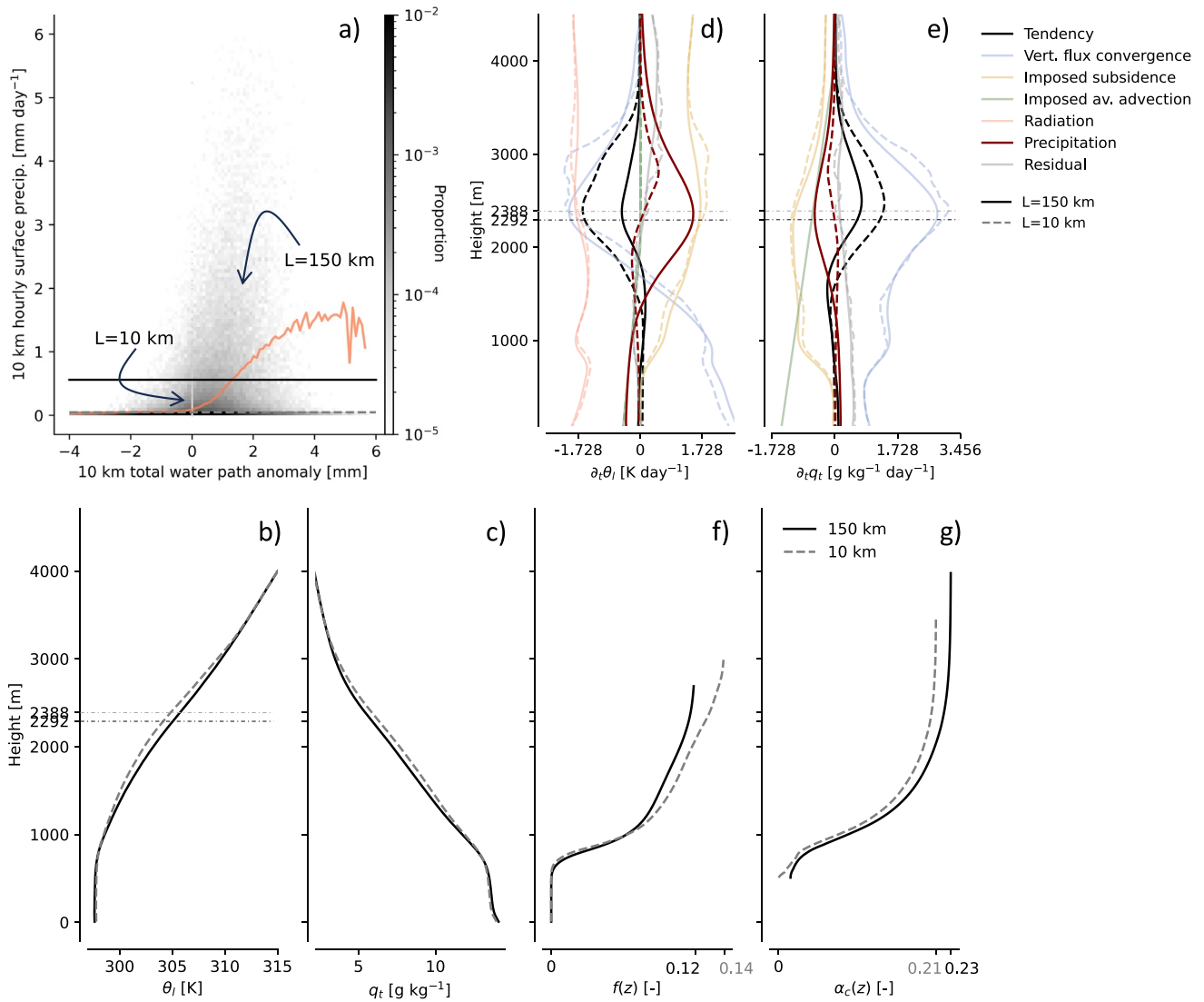


**Figure 2.** (a) Joint histogram (shading) of the total water path fluctuation  $I'$  around the horizontal domain mean, and rain rate  $P_s$ , averaged over  $10 \times 10 \text{ km}^2$  sub-domains and 1h, in all mesoscale-domain simulations ( $L = 150 \text{ km}$ ). The orange line indicates the ensemble-mean  $P_s$  over each  $I'$ -bin, light-gray scatter at  $I' = 0$  indicates  $P_s$  in the small-domain ensemble ( $L = 10 \text{ km}$ ), and horizontal lines indicate the ensemble-mean  $P_s$  in mesoscale domains (black, unbroken) and small domains (gray, broken). (b) and (c) Ensemble-averaged  $\theta_t$  and  $q_t$  profiles for mesoscale-domain (black, unbroken) and small-domain (gray, broken) simulations. (d) and (e) Terms contributing to horizontally averaged heating  $\partial\theta_t/\partial t$  and moistening  $\partial q_t/\partial t$ , with the most different terms between ensembles - the tendency (black) and precipitation heating/drying (maroon) - emphasized. (f) and (g) cumulative contribution of model levels below  $z$  toward the cloud cover  $f$  at  $z$  ( $f(z)$ ) and albedo in cloudy columns  $\alpha_c$  at  $z$  ( $\alpha_c(z)$ ), until the height where  $f(z) = f$  and  $\alpha_c(z) = \alpha_c$  (x-axis ticks). In Figures (b–g), the results are averaged over 30–54 hr.

across the ensemble. As  $I'$  rises above 0, the hourly subdomain-averaged  $P_s$  sharply increases too (orange line Figure 2a), in a shallow analogy of the well-established relationship between  $I$  and  $P_s$  across the tropics (Bretherton et al., 2004; Nuijens et al., 2009; Radtke et al., 2023): More than 80% of the precipitation in the mesoscale-domain ensemble falls in sub-domains where  $I' > 0$ . The small-domain simulations cannot produce the mesoscale circulations and cold pools needed to create these mesoscale moisture fluctuations ( $I' = 0$  by construction). Their low, 10-km scale  $P_s$  is indicated by light-gray scatter in Figure 2a).

Two effects of the additional precipitation modify the mesoscale-domain simulations' mean thermodynamic structure. First, the precipitating mesoscale systems heat the upper regions of the mesoscale-domain cloud layer relative to small domains (Figures 2b and 2d), in line with simple models and small-domain LES (Albrecht, 1993; Bretherton et al., 2013; Stevens & Seifert, 2008). A mesoscale, cloud-layer weak-temperature-gradient constraint (Bretherton & Blossey, 2017; Janssens et al., 2022, 2024) efficiently communicates this latent heating from the

mesoscale systems across the mesoscale domains, resulting in weaker, lower domain-wide inversions than in small domains (y-ticks in Figure 2b). Second, the larger precipitation fluxes in mesoscale domains sediment additional moisture from their cloud layers, reducing horizontally averaged  $q_t$  (Figures 2c and 2e). The combined warming and drying lowers the cloud-layer relative humidity by 6% in the mesoscale-domain ensemble, relative to the small-domain ensemble (Figure S1 in Supporting Information S1).

The drier, warmer mesoscale-domain cloud layers have a slightly lower  $f$  than small domains (Figure 2f). The cumulative, height-wise contribution to  $f$  ( $f(z)$ ) attributes this reduction to the upper cloud layer (from around 1,000 m), where both the drying and stabilization is felt, and to the lower inversion, where less additional clouds develop. Yet, the larger convective systems which develop in the moist regions of mesoscale domains are structurally geometrically thicker, more adiabatic and more liquid-water laden than the smaller clouds in the small domains (Plank, 1969; Stephens, 1978; Benner & Curry, 1998; Zhao & Di Girolamo, 2007; Feingold et al., 2017, see Text S1 in Supporting Information S1). Hence, the organized convection in mesoscale domains has a slightly larger  $\alpha_c$  than the unorganized convection in small domains (Alinaghi et al., 2023), both at a given height, and over a deeper layer (Figure 2g).

In all, compared to small domains, self-organisation in mesoscale domains gives both larger cloud structures (larger  $L_c$ ) with larger  $\alpha_c$ , and larger cloud-free areas (larger  $L_o$ ) and reductions in  $f$ . Put differently, mesoscale dynamics concentrate cloudiness in fewer, larger structures, which live at the expense of the many, smaller clouds (Figure S2 in Supporting Information S1).

### 3.2. Top-Of-Atmosphere Radiative Fluxes

In each ensemble, we next evaluate the top-of-atmosphere net radiation

$$N = -F_{s,c}^\uparrow - F_{l,c}^\uparrow + C_s + C_l, \quad (1)$$

decomposed into clear-sky net outgoing shortwave and longwave radiative fluxes ( $-F_{s,c}^\uparrow$  and  $-F_{l,c}^\uparrow$ ), and short-wave and longwave cloud-radiative effects ( $C_s$  and  $C_l$ ). These horizontally averaged terms are constructed from column-wise all- and clear-sky radiative fluxes, evaluated at runtime by the LES's radiative transfer model (Iacono et al., 2008).

Figure 3a) plots the difference in each component between all mesoscale and small-domain simulations, that is,  $\Delta N = N_{\text{meso}} - N_{\text{small}}$ . It shows a small ensemble-averaged  $\Delta N = -0.51 \text{ W m}^{-2}$ , that is, a cooling in mesoscale-domain simulations. The mesoscale domains cool through larger clear-sky longwave cooling ( $-\Delta F_{l,c}^\uparrow = -1.01 \text{ W m}^{-2}$ ) and a smaller  $C_l$  warming ( $\Delta C_l = -0.31 \text{ W m}^{-2}$ ), which together outweigh a smaller mesoscale-domain cooling from  $C_s$  ( $\Delta C_s = 0.82 \text{ W m}^{-2}$ ).

The changes in all three terms can be understood in terms of the mean state's differences presented in Figure 2. First, writing  $C_s = F_s^\downarrow f \alpha_c$ , where  $F_s^\downarrow$  is the TOA downwards shortwave radiative flux, we primarily attribute  $\Delta C_s \approx F_s^\downarrow (\alpha_c \Delta f + f \Delta \alpha_c)$  to the reduction in  $f$  in mesoscale domains, which outweigh the increases in  $\alpha_c$  (Figure 3b, left bracket). Second, modeling  $C_l \approx -f \lambda_p (T_c - T_s)$  (e.g., McKim et al., 2024), with  $T_c$  and  $T_s$  the average cloud-layer and surface temperatures, and  $\lambda_p$  an appropriate longwave clear-sky feedback,  $\Delta C_l \approx -\lambda_p ((T_c - T_s) \Delta f + f \Delta T_c)$  is also mostly due to the reductions in  $f$  (Figure 3b, right bracket). Finally, almost the entire increase in the mesoscale-domain clear-sky longwave cooling can be explained by their cloud-layer drying, in line with Fildier et al. (2023). That is, given the domain-averaged  $I$ ,  $-\Delta F_{l,c}^\uparrow \approx -\partial F_{l,c}^\uparrow / \partial I \times \Delta I$ , as estimated by linear regression (Figure 3b, central bracket). This result echoes how mean drying in the presence of aggregated deep convection allows the clear skies of such domains to radiate more efficiently to space than in disaggregated situations (e.g., Bony et al., 2020; Bretherton et al., 2005), though the simulated shallow convective difference is weaker.

### 4. Mesoscale Self-Organisation Weakly Modifies a Small Trade Cumulus Feedback

In all, self-organisation in mesoscale domains gives a small, systematic cooling compared to small domains, from reductions in  $f$ , increases in  $\alpha_c$  and reductions in  $I$ . Yet, the resultant modifications of the radiation budget's two

Contribution to top-of-atmosphere radiative budget differences

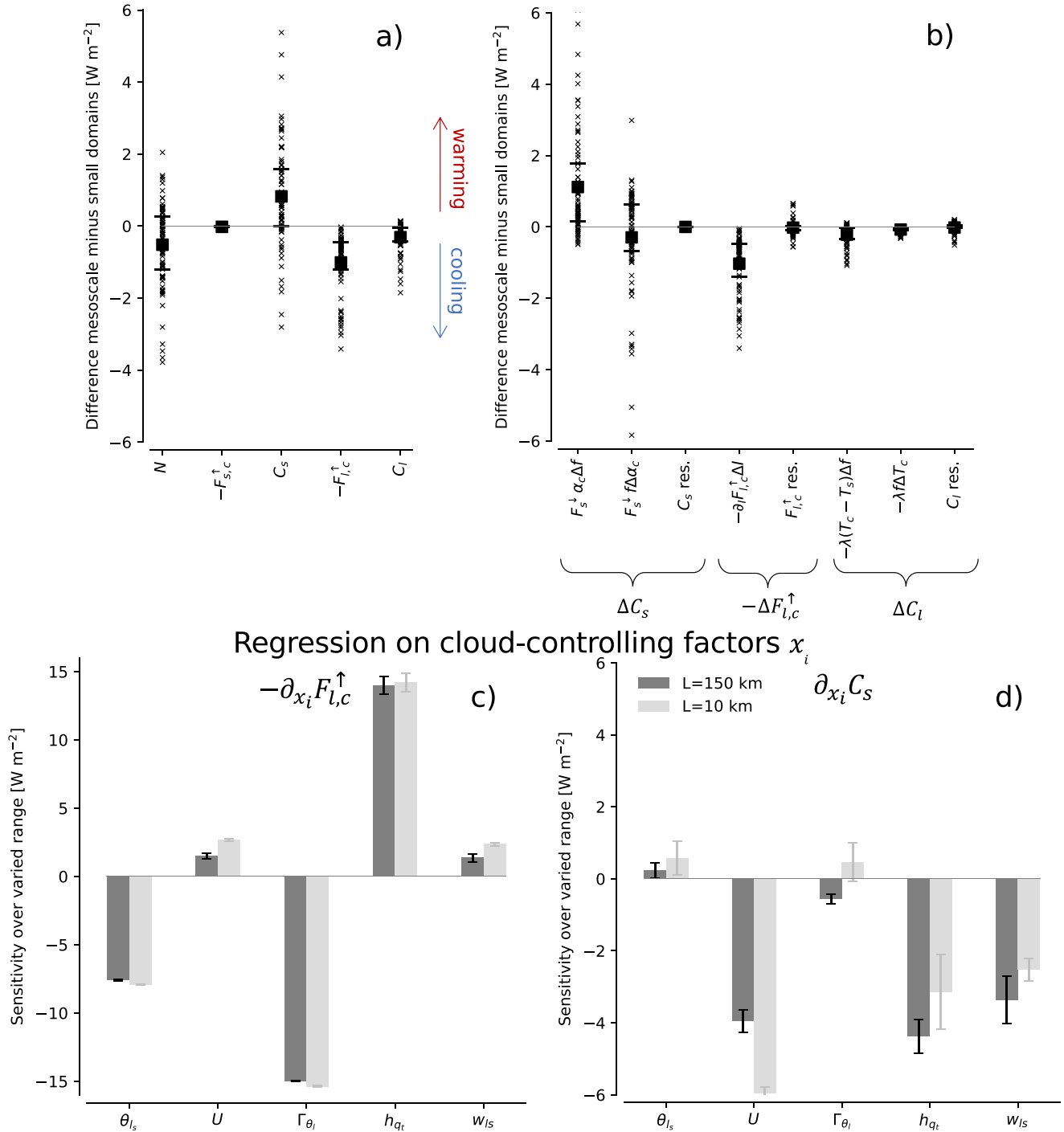


**Figure 3.** (a) Differences in TOA net radiation between each mesoscale-domain and small-domain simulation ( $\Delta N$ , crosses) and its contributions from shortwave and longwave clear-sky fluxes ( $-F_{s,c}^{\uparrow}$  and  $-F_{l,c}^{\uparrow}$ ) and cloud-radiative effects ( $C_s$  and  $C_l$ ). Squares and horizontal bars mark the mean and inter-quartile range over the ensemble members. (b) As in (a), with  $\Delta C_s$ ,  $-\Delta F_{l,c}^{\uparrow}$  and  $\Delta C_l$  broken down by the mean state changes in cloud cover  $f$ , cloud-albedo  $\alpha_c$ , vertically integrated total water specific humidity  $I$  and cloud-layer temperature  $T_c$  (see text). Residuals in  $\Delta C_s$ ,  $-\Delta F_{l,c}^{\uparrow}$  and  $\Delta C_l$  when these contributions are summed are marked “res”. (c) and (d) Linear least squares regression coefficients of  $C_s$  (c) and  $F_{l,c}^{\uparrow}$  (d) on individual cloud-controlling factors, in mesoscale ( $L = 150$  km, dark) and small ( $L = 10$  km, light) domains. All variables are averaged between 30 and 54 hr.

components that are most sensitive to domain size,  $F_{l,c}^\dagger$  and  $C_s$ , usually remain weak compared to variability in  $F_{l,c}^\dagger$  and  $C_s$  associated with changes in the imposed CCFs  $x = [\theta_l, U, \Gamma_{\theta_l}, h_{q_l}, w_{ls}]$ . To show this, we compute the sensitivities  $\partial_{x_i} F_{l,c}^\dagger$  and  $\partial_{x_i} C_s$  (we denote partial differentiation  $Y$  to  $x_i$  as  $\partial_{x_i} Y$ ). We calculate  $\partial_{x_i} C_s$  and  $\partial_{x_i} F_{l,c}^\dagger$  by averaging  $C_s$  and  $F_{l,c}^\dagger$  over 30–54 hr, and linearly regressing them on  $x_i$  in ensemble members where  $x_i$  is varied, while all other CCFs are kept constant at their central value (“sweeps” in Jansson et al., 2023). We then multiply the sensitivities by  $x_i$ 's varied range, giving variability in  $C_s$  and  $F_{l,c}^\dagger$  due to climatologically representative variations in  $x_i$ .

Figure 3c shows the familiar, strong cooling response of  $F_{l,c}^\dagger$  to warming the entire tropical atmosphere by a roughly constant amount ( $\theta_l$ , i.e. the Planck response) and increasing  $\Gamma_{\theta_l}$  (the lapse rate response), and the warming response to increasing  $q_l$  (the water vapor response). The latter is measured both directly (by increasing  $h_{q_l}$ ) and indirectly, by (a) raising  $U$ , which boosts the surface moisture fluxes, moistening the boundary layer, and (b) making  $w_{ls}$  more positive, which reduces the vertical advective drying of large-scale subsidence (see Figure S3 in Supporting Information S1). The largest three sensitivities are an order of magnitude larger than differences between mesoscale and small domains. That is, across today's trade-wind CCF climatology, the response of clear-sky radiation to changes in variables that also will change with tropical warming ( $\theta_l, \Gamma_{\theta_l}, h_{q_l}$ ), is insensitive to whether shallow convection is self-organized at mesoscales or not.

The sensitivities  $\partial_{x_i} C_s$  (Figure 3d) are also generally larger than differences between mesoscale and small domains, although mesoscale-domain  $C_s$  is structurally less sensitive to changes in  $U$ , and more sensitive to changes in  $h_{q_l}$  and  $w_{ls}$ . Yet, focusing on  $\partial_{\theta_l} C_s$  and  $\partial_{\Gamma_{\theta_l}} C_s$ , the largest two contributors to observed variability in trade cumulus  $C_s$  (Scott et al., 2020) and its response to warming (Myers et al., 2021), both mesoscale and small domains agree that they are near-zero.

The predicted  $\partial_{\theta_l} C_s$  ( $0.07 \text{ Wm}^{-2} \text{ K}^{-1}$  and  $0.11 \text{ Wm}^{-2} \text{ K}^{-1}$  for mesoscale and small domains respectively) also align with satellite observations over the North-Atlantic trades ( $0.11$ – $0.13 \text{ Wm}^{-2} \text{ K}^{-1}$ , Scott et al., 2020; Cesana & Del Genio, 2021), as do the simulated reductions in  $f$  ( $1\% \text{ K}^{-1}$ , against  $1\%$ – $2\% \text{ K}^{-1}$  in Mieslinger et al., 2019; Cesana et al., 2019). Contrarily, the simulated  $\partial_{\Gamma_{\theta_l}} C_s$  ( $-0.48$  and  $0.65 \text{ Wm}^{-2}$  for mesoscale and small domains) are an order of magnitude smaller than the sensitivity of satellite-derived radiative fluxes to reanalysis-inferred Estimated Inversion Strength (EIS, Wood & Bretherton, 2006):  $-5.44 \text{ Wm}^{-2}$  over the EIS range implied by our  $\Gamma_{\theta_l}$  sweep (Scott et al., 2020). In the simulations, the smaller  $\partial_{\Gamma_{\theta_l}} C_s$  arises from offsetting effects: Stabilizing the free troposphere lowers and strengthens the trade inversion (e.g., Bellon & Stevens, 2012, Figure S4c, S4h in Supporting Information S1), reducing the shallow convection's depth and  $\alpha_c$ , but increasing inversion cloudiness and  $f$  (Figure S5c, S5h in Supporting Information S1). Scott et al. (2020) suggest that raising the EIS in trade-cumulus regimes increases both  $f$  and  $\alpha_c$ , likely because they do not find that increasing EIS reduces cloud top height (their Figure S11b in Supporting Information S1). This places the observations in conflict with bulk theory and our simulations. Since Scott et al. (2020) identify EIS as the second strongest control on  $C_s$  in trade-cumulus regions, resolving this inconsistency is warranted.

The fact that mesoscale self-organisation only weakly modifies  $\partial_{x_i} F_{l,c}^\dagger$  and  $\partial_{x_i} C_s$ , explains why both small-domain LESs and CCF-observation frameworks project the same weak trade cumulus feedback  $\lambda_t = \partial_{x_i} C_s \times \partial_{T_s} x_i$ : Since  $\partial_{x_i} C_s$  are similar to what is observed in both our mesoscale- and small-domain LESs, were we to multiply them with sensitivities of  $x_i$  to surface warming ( $\partial_{T_s} x_i$ ), for example, from climate models under a scenario of climate change, our mesoscale- and small-domain ensembles would project similar, small estimates of the trade-cumulus feedback as studies that take this approach based on the observed  $\partial_{x_i} C_s$  (Ceppi & Nowack, 2021; Cesana & Del Genio, 2021; Myers et al., 2021) (though there would be slightly less cooling from the smaller sensitivity to  $\Gamma_{\theta_l}$ ).

## 5. A Symmetry Hypothesis for Mesoscale Cloud-Circulation Coupling

In essence, our results suggest that self-generated mesoscale circulations, be they through moisture-convection feedbacks or cold pool dynamics, do not greatly modify the mean  $C_s$  in fields of shallow cumuli. This is perhaps somewhat surprising, given strong observed correlations between mesoscale vertical motion and

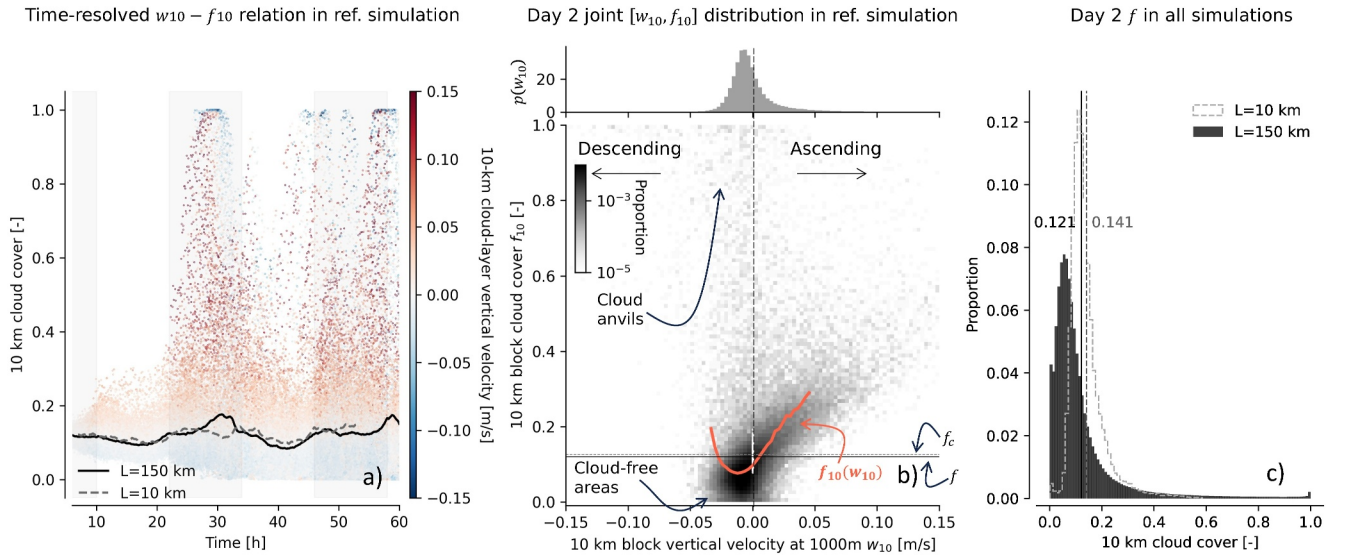


**Figure 4.** (a) Time-evolution of cloud cover  $f_{10}$  (y-axis) and cloud-layer (1,000 m) vertical motion  $w_{10}$  (colors) averaged over  $10 \times 10 \text{ km}^2$  sub-domains in the Cloud Botany reference simulation, with the mesoscale ( $L = 150 \text{ km}$ ) and small ( $L = 10 \text{ km}$ ) domain-averaged  $f$  (lines). (b) Joint histogram of  $w_{10}$  and  $f_{10}$  and marginal density function  $p(w_{10})$  in reference simulation between 30 and 54 hr (day 2, shading as Figure 2), with white scatter indicating small-domain  $f$  at  $w_{10} = 0$ , horizontal lines indicating mesoscale-domain and small-domain  $f$  ( $f, f_c$ ), and the orange line indicating  $f_{10}$  averaged over a  $w$ -bin,  $f_{10}(w_{10})$ . (c) Histogram of day 2- $f$  in all simulations of the mesoscale-domain ensemble ( $L = 150 \text{ km}$ , black) and small-domain ensemble ( $L = 10 \text{ km}$ , gray outline). Vertical lines mark the mean  $f$  across both ensembles.

cloudiness in the trades (George et al., 2021; Vogel et al., 2022). Such correlations are present in our ensemble too: In mesoscale-domain simulations, the  $10 \times 10 \text{ km}^2$ -averaged  $f$  ( $f_{10}$ ) rises almost proportionally with  $10 \times 10 \text{ km}^2$ -averaged  $w$  evaluated at 1,000 m ( $w_{10}$ ) (Figures 4a and 4b). Yet, because mesoscale variability in active cloudiness generates  $w_{10}$  (Janssens et al., 2024), ascending sub-domains with large (convective) cloudiness must be compensated by descending sub-domains with low cloudiness, for the circulations to exist at all. In our simulations, these opposing effects almost cancel: Expressing the  $w_{10}$ -bin averaged  $f_{10}$  (orange line, Figure 4b) as

$$f_{10}(w_{10}) = f_c + f'_{10}(w_{10}), \quad (2)$$

where  $f_c$  is the ( $w_{10}$ -independent) small-domain simulation  $f$ , then the contribution to  $f$  from mesoscale cloud-circulation coupling ( $f'_{10}(w_{10})$ , weighted by the marginal probability density function of  $w_{10}$ ,  $p(w_{10})$ ) is near-zero:

$$f = f_c + \int_{-\infty}^{\infty} p(w_{10}) f'_{10}(w_{10}) dw_{10} \approx f_c. \quad (3)$$

So, in these simulations, mesoscale circulations give large, skewed variability in 10 km-scale  $f$  across a mesoscale domain at any time (Figure 4a), but small changes in 150 km-scale  $f$  relative to this variability, both in a given mesoscale-domain simulation (Figure 4b) and across the ensemble (Figure 4c). That is, the ascending and descending branches of mesoscale circulations are *nearly symmetric* in their opposing effect on  $f$ , and  $C_s$ .

The emergence of this cloud-circulation symmetry is not trivial to us. It depends on  $f'_{10}(w)$ , which rises linearly where  $w_{10} > 0$ , as larger active cloud areas give larger uncompensated vertical mass fluxes (Janssens et al., 2024; Lamer et al., 2015; Sakradzija & Klingebiel, 2020). But  $f'_{10}(w)$  becomes non-linear where  $w_{10} < 0$ , due to both passive (i.e., non- $w_{10}$ -controlled) cloud anvils flowing from convecting regions and cloud-free sub-domains with strong compensating subsidence (Figure 4b). Somehow, the ascending and descending motions are organized such that scaling  $f'_{10}(w)$  by  $p(w_{10})$  and integrating over  $w_{10}$  nearly averages these effects away.

The cloud-circulation symmetry may be exaggerated in our doubly periodic LESs, where  $w$  must vanish at the domain scale. Yet also in nature, once the coherent vertical motion of the large-scale tropical circulation is subtracted, entire trade-wind regimes do not exhibit a mean vertical cloud-layer velocity. Hence, the symmetry in these simulations emphasizes that circulations of scales smaller than the entire trades can only modify  $C_s$  if their

ascending branches asymmetrically affect  $f$  or  $\alpha_c$  with respect to their descending branches. Averaged over our ensemble, these effects are small ( $\sim 2\%$ , Figures 2f and 2g) relative to their imprint on mesoscale variability ( $\sim 20\%$ , Figure 4c), and they are buffered by both the opposite-sign responses of  $f$  or  $\alpha_c$  and the increased longwave cooling (Figure 3b). The resultant TOA net radiation changes ( $-0.5 \text{ W m}^{-2}$ ) are thus small, relative to variability induced by larger-scale cloud-controlling factors (Figures 3c and 3d).

Of course, this discussion hinges on the realism of idealized LESs, which retain several biases. The ensemble-averaged  $f$  (0.12) is substantially lower than the EUREC<sup>4</sup>A average (0.42, Mieslinger et al., 2022). The relative importance of  $C_l$  (ensemble-average  $1.1 \text{ W m}^{-2}$ ) to  $C_s$  ( $-7.2 \text{ W m}^{-2}$ ) is likely underestimated (Schulz & Stevens, 2023). Our environmental control factors are simpler and sparser than in nature. The simulated mesoscale dynamics are sensitive to arbitrary model choices (Janssens et al., 2023; Li et al., 2015); simulations at half (50 m) the horizontal grid spacing in four ensemble members produce slightly more clouds and 15% larger  $C_s$ , though their organisation develops at a similar time scale at finer resolution. Finally, even our doubly periodic mesoscale domains are too small and idealized to simulate cloud structures and circulations which grow from pre-existing disturbances to scales of  $>700 \text{ km}$  in more realistic setups (Janssens et al., 2024). What these LESs do instead, is pose the hypothesis that mesoscale circulations are nearly symmetric in their effects on the TOA radiation balance, and thus will not substantially alter contemporary estimates of a weak trade cumulus contribution to the cloud feedback on warming. We now require results akin to Figure 4b from more realistically configured simulations and observations, to truly understand whether the intrinsic tendency of trade cumuli to self-organize is just beautiful and striking, or whether it impacts global climate.

### Data Availability Statement

The mesoscale-domain and small-domain Cloud Botany simulations are hosted at the German Climate Computing Center (DKRZ) and are freely available through the EUREC<sup>4</sup>A intake catalog ([https://howto.eurec4a.eu/botany\\_daes.html](https://howto.eurec4a.eu/botany_daes.html)). The metrics underlying Figure 1 have been computed with the Cloudmetrics code package v0.2.0 (Janssens & Denby, 2022). These metrics, and all code required to produce the figures and data herein are publicly available (Janssens, 2024). Finally, the meteorological cloud-radiative kernels computed by Scott et al. (2020) have been retrieved from [https://github.com/tamyers87/meteorological\\_cloud\\_radiative\\_kernels](https://github.com/tamyers87/meteorological_cloud_radiative_kernels). We thank these authors for making their data publicly available.

### References

- Albrecht, B. A. (1993). Effects of precipitation on the thermodynamic structure of the trade wind boundary layer. *Journal of Geophysical Research*, 98(D4), 7327–7337. <https://doi.org/10.1029/93jd00027>
- Alinaghi, P., Janssens, M., Choudhury, G., Goren, T., Siebesma, A. P., & Glassmeier, F. (2023). Shallow cumulus cloud fields are optically thicker when they are more clustered. *Quarterly Journal of the Royal Meteorological Society*, 150(763), 3566–3577. <https://doi.org/10.1002/qj.4783>
- Alinaghi, P., Siebesma, P., Jansson, F., Janssens, M., & Glassmeier, F. (2024). External drivers and mesoscale self-organization of shallow cold pools in the trade-wind regime. *Authorea Preprints*.
- Bellon, G., & Stevens, B. (2012). Using the sensitivity of large-eddy simulations to evaluate atmospheric boundary layer models. *Journal of the Atmospheric Sciences*, 69(5), 1582–1601. <https://doi.org/10.1175/jas-d-11-0160.1>
- Benner, T. C., & Curry, J. A. (1998). Characteristics of small tropical cumulus clouds and their impact on the environment. *Journal of Geophysical Research*, 103(D22), 28753–28767. <https://doi.org/10.1029/98jd02579>
- Blossey, P. N., Bretherton, C. S., Zhang, M., Cheng, A., Endo, S., Heus, T., et al. (2013). Marine low cloud sensitivity to an idealized climate change: The CGILS LES intercomparison. *Journal of Advances in Modeling Earth Systems*, 5(2), 234–258. <https://doi.org/10.1002/jame.20025>
- Bony, S., & Dufresne, J.-L. (2005). Marine boundary layer clouds at the heart of tropical cloud feedback uncertainties in climate models. *Geophysical Research Letters*, 32(20). <https://doi.org/10.1029/2005gl023851>
- Bony, S., Semie, A., Kramer, R. J., Soden, B., Tompkins, A. M., & Emanuel, K. A. (2020). Observed modulation of the tropical radiation budget by deep convective organization and lower-tropospheric stability. *AGU Advances*, 1(3), e2019AV000155. <https://doi.org/10.1029/2019av000155>
- Bretherton, C. S. (2015). Insights into low-latitude cloud feedbacks from high-resolution models. *Philosophical Transactions of the Royal Society A: Mathematical, Physical & Engineering Sciences*, 373(2054), 20140415. <https://doi.org/10.1098/rsta.2014.0415>
- Bretherton, C. S., & Blossey, P. N. (2017). Understanding mesoscale aggregation of shallow cumulus convection using large-eddy simulation. *Journal of Advances in Modeling Earth Systems*, 9(8), 2798–2821. <https://doi.org/10.1002/2017ms000981>
- Bretherton, C. S., Blossey, P. N., & Jones, C. R. (2013). Mechanisms of marine low cloud sensitivity to idealized climate perturbations: A single-LES exploration extending the CGILS cases. *Journal of Advances in Modeling Earth Systems*, 5(2), 316–337. <https://doi.org/10.1002/jame.20019>
- Bretherton, C. S., Blossey, P. N., & Khairoutdinov, M. (2005). An energy-balance analysis of deep convective self-aggregation above uniform SST. *Journal of the Atmospheric Sciences*, 62(12), 4273–4292. <https://doi.org/10.1175/jas3614.1>
- Bretherton, C. S., McCaa, J. R., & Grenier, H. (2004). A new parameterization for shallow cumulus convection and its application to marine subtropical cloud-topped boundary layers. Part I: Description and 1D results. *Monthly Weather Review*, 132(4), 864–882. [https://doi.org/10.1175/1520-0493\(2004\)132<0864:anfisc>2.0.co;2](https://doi.org/10.1175/1520-0493(2004)132<0864:anfisc>2.0.co;2)

### Acknowledgments

MJ thanks Jordi Vilà and Raphaela Vogel for fruitful feedback on an earlier version of this manuscript. APS and FJ acknowledge support from the European Union's Horizon 2020 research and innovation program under grant agreement no. 820829 (CONSTRAIN project). FG and PA acknowledge support from The Branco Weiss Fellowship - Society in Science, administered by ETH Zürich. FG further acknowledges funding by the European Union (ERC, MesoClou, 101117462). Views and opinions expressed are however those of the author(s) only and do not necessarily reflect those of the European Union or the European Research Council Executive Agency. Neither the European Union nor the granting authority can be held responsible for them. This research used computational resources of Fugaku provided by RIKEN through the HPCI System Research Project (Project ID: hp200321), and the Dutch National Supercomputer Snellius, administered by SURF. We also thank DKRZ for hosting the Cloud Botany data set under project ID bm1349.

- Brueck, M., Nuijens, L., & Stevens, B. (2015). On the seasonal and synoptic time-scale variability of the North Atlantic trade wind region and its low-level clouds. *Journal of the Atmospheric Sciences*, 72(4), 1428–1446. <https://doi.org/10.1175/jas-d-14-0054.1>
- Ceppi, P., & Nowack, P. (2021). Observational evidence that cloud feedback amplifies global warming. *Proceedings of the National Academy of Sciences*, 118(30), e2026290118. <https://doi.org/10.1073/pnas.2026290118>
- Cesana, G., & Del Genio, A. D. (2021). Observational constraint on cloud feedbacks suggests moderate climate sensitivity. *Nature Climate Change*, 11(3), 213–218. <https://doi.org/10.1038/s41558-020-00970-y>
- Cesana, G., Del Genio, A. D., Ackerman, A. S., Kelley, M., Elsaesser, G., Fridlind, A. M., et al. (2019). Evaluating models' response of tropical low clouds to sst forcings using calipso observations. *Atmospheric Chemistry and Physics*, 19(5), 2813–2832. <https://doi.org/10.5194/acp-19-2813-2019>
- Coakley, J. A., & Chylek, P. (1975). The two-stream approximation in radiative transfer: Including the angle of the incident radiation. *Journal of the Atmospheric Sciences*, 32(2), 409–418. [https://doi.org/10.1175/1520-0469\(1975\)032<0409:tsair>2.0.co;2](https://doi.org/10.1175/1520-0469(1975)032<0409:tsair>2.0.co;2)
- Dauhut, T., Couvreux, F., Bouniol, D., Beucher, F., Volkmer, L., Pörtge, V., et al. (2023). Flower trade-wind clouds are shallow mesoscale convective systems. *Quarterly Journal of the Royal Meteorological Society*, 149(750), 325–347. <https://doi.org/10.1002/qj.4409>
- Feingold, G., Balsells, J., Glassmeier, F., Yamaguchi, T., Kazil, J., & McComiskey, A. (2017). Analysis of albedo versus cloud fraction relationships in liquid water clouds using heuristic models and large eddy simulation. *Journal of Geophysical Research: Atmospheres*, 122(13), 7086–7102. <https://doi.org/10.1002/2017jd026467>
- Fildier, B., Muller, C., Pincus, R., & Fueglistaler, S. (2023). How moisture shapes low-level radiative cooling in subsidence regimes. *AGU Advances*, 4(3). <https://doi.org/10.1029/2023AV000880>
- George, G., Stevens, B., Bony, S., Klingebiel, M., & Vogel, R. (2021). Observed impact of mesoscale vertical motion on cloudiness. *Journal of the Atmospheric Sciences*, 78(8), 2413–2427. <https://doi.org/10.1175/jas-d-20-0335.1>
- George, G., Stevens, B., Bony, S., Vogel, R., & Naumann, A. K. (2023). Widespread shallow mesoscale circulations observed in the trades. *Nature Geoscience*, 16(7), 584–589. <https://doi.org/10.1038/s41561-023-01215-1>
- Iacono, M. J., Delamere, J. S., Mlawer, E. J., Shephard, M. W., Clough, S. A., & Collins, W. D. (2008). Radiative forcing by long-lived greenhouse gases: Calculations with the AER radiative transfer models. *Journal of Geophysical Research*, 113(D13). <https://doi.org/10.1029/2008jd009944>
- Janssens, M. (2024). Supporting data for manuscript “Symmetry in mesoscale circulations explains weak impact of trade cumulus self-organisation on the radiation budget in large-eddy simulations” (v1.1) [Collection]. *Zenodo*. <https://doi.org/10.5281/zenodo.14011425>
- Janssens, M., & Denby, L. (2022). cloudsci/cloudmetrics [Software]. *Zenodo*. <https://doi.org/10.5281/zenodo.7506966>
- Janssens, M., George, G., Schulz, H., Couvreux, F., & Bouniol, D. (2024). Shallow convective heating in weak temperature gradient balance explains mesoscale vertical motions in the trades. *ESS Open Archive*. <https://doi.org/10.22541/essoar.171415887.72921250/v1>
- Janssens, M., Vilà-Guerau De Arellano, J., Scheffer, M., Antonissen, C., Siebesma, A. P., & Glassmeier, F. (2021). Cloud patterns in the trades have four interpretable dimensions. *Geophysical Research Letters*, 48(5), e2020GL091001. <https://doi.org/10.1029/2020gl091001>
- Janssens, M., Vilà-Guerau-De Arellano, J., Van Heerwaarden, C. C., De Roode, S. R., Siebesma, A. P., & Glassmeier, F. (2022). Nonprecipitating shallow cumulus convection is intrinsically unstable to length scale growth. *Journal of the Atmospheric Sciences*, 80(3), 849–870.
- Janssens, M., Vilà-Guerau De Arellano, J., Van Heerwaarden, C. C., Van Stratum, B. J., De Roode, S. R., Siebesma, A. P., & Glassmeier, F. (2023). The time scale of shallow convective self-aggregation in large-eddy simulations is sensitive to numerics. *Journal of Advances in Modeling Earth Systems*, 15(1), e2022MS003292. <https://doi.org/10.1029/2022ms003292>
- Jansson, F., Janssens, M., Grönqvist, J. H., Siebesma, P., Glassmeier, F., Attema, J. J., et al. (2023). Cloud botany: Shallow cumulus clouds in an ensemble of idealized large-domain large-eddy simulations of the trades. *Journal of Advances in Modeling Earth Systems*, 10(11), e2023MS003796. <https://doi.org/10.1029/2023ms003796>
- Klein, S. A., Hall, A., Norris, J. R., & Pincus, R. (2017). Low-cloud feedbacks from cloud-controlling factors: A review. In R. Pincus, M. Winker, S. Bony, & B. Stevens (Eds.), *Shallow clouds, water vapor, circulation, and climate sensitivity* (pp. 135–157). Springer.
- Lamaakel, O., & Matheou, G. (2022). Organization development in precipitating shallow cumulus convection: Evolution of turbulence characteristics. *Journal of the Atmospheric Sciences*, 79(9), 2419–2433. <https://doi.org/10.1175/jas-d-21-0334.1>
- Lamer, K., Kollias, P., & Nuijens, L. (2015). Observations of the variability of shallow trade wind cumulus cloudiness and mass flux. *Journal of Geophysical Research: Atmospheres*, 120(12), 6161–6178. <https://doi.org/10.1002/2014jd022950>
- Li, Z., Zuidema, P., Zhu, P., & Morrison, H. (2015). The sensitivity of simulated shallow cumulus convection and cold pools to microphysics. *Journal of the Atmospheric Sciences*, 72(9), 3340–3355. <https://doi.org/10.1175/jas-d-14-0099.1>
- McKim, B., Bony, S., & Dufresne, J.-L. (2024). Weak anvil cloud area feedback suggested by physical and observational constraints. *Nature Geoscience*, 17(5), 1–6. <https://doi.org/10.1038/s41561-024-01414-4>
- Mieslinger, T., Horváth, Á., Buehler, S. A., & Sakradzija, M. (2019). The dependence of shallow cumulus macrophysical properties on large-scale meteorology as observed in ASTER imagery. *Journal of Geophysical Research: Atmospheres*, 124(21), 11477–11505. <https://doi.org/10.1029/2019jd030768>
- Mieslinger, T., Stevens, B., Kölling, T., Brath, M., Wirth, M., & Buehler, S. A. (2022). Optically thin clouds in the trades. *Atmospheric Chemistry and Physics*, 22(10), 6879–6898. <https://doi.org/10.5194/acp-22-6879-2022>
- Myers, T. A., & Norris, J. R. (2016). Reducing the uncertainty in subtropical cloud feedback. *Geophysical Research Letters*, 43(5), 2144–2148. <https://doi.org/10.1002/2015gl067416>
- Myers, T. A., Scott, R. C., Zelinka, M. D., Klein, S. A., Norris, J. R., & Caldwell, P. M. (2021). Observational constraints on low cloud feedback reduce uncertainty of climate sensitivity. *Nature Climate Change*, 11(6), 501–507. <https://doi.org/10.1038/s41558-021-01039-0>
- Narenpitak, P., Kazil, J., Yamaguchi, T., Quinn, P. K., & Feingold, G. (2021). From sugar to flowers: A transition of shallow cumulus organization during ATOMIC. *Journal of Advances in Modeling Earth Systems*, 13(10), e2021MS002619. <https://doi.org/10.1029/2021ms002619>
- Nuijens, L., Stevens, B., & Siebesma, A. P. (2009). The environment of precipitating shallow cumulus convection. *Journal of the Atmospheric Sciences*, 66(7), 1962–1979. <https://doi.org/10.1175/2008jas2841.1>
- O, K.-T., Wood, R., & Tseng, H. (2018). Deeper, precipitating PBLs associated with optically thin veil clouds in the Sc-Cu transition. *Geophysical Research Letters*, 45(10), 5177–5184. <https://doi.org/10.1029/2018gl077084>
- Plank, V. G. (1969). The size distribution of cumulus clouds in representative Florida populations. *Journal of Applied Meteorology and Climatology*, 8(1), 46–67. [https://doi.org/10.1175/1520-0450\(1969\)008<0046:tsdocc>2.0.co;2](https://doi.org/10.1175/1520-0450(1969)008<0046:tsdocc>2.0.co;2)
- Radtke, J., Mauritsen, T., & Hohenegger, C. (2021). Shallow cumulus cloud feedback in large eddy simulations—bridging the gap to storm-resolving models. *Atmospheric Chemistry and Physics*, 21(5), 3275–3288. <https://doi.org/10.5194/acp-21-3275-2021>
- Radtke, J., Vogel, R., Ament, F., & Naumann, A. K. (2023). Spatial organisation affects the pathway to precipitation in simulated trade-wind convection. *Autor*. <https://doi.org/10.22541/essoar.167979635.58663858/v1>

- Sakradzija, M., & Klingebiel, M. (2020). Comparing ground-based observations and a large-eddy simulation of shallow cumuli by isolating the main controlling factors of the mass flux distribution. *Quarterly Journal of the Royal Meteorological Society*, *146*(726), 254–266. <https://doi.org/10.1002/qj.3671>
- Schulz, H., & Stevens, B. (2023). On the representation of shallow convection in the trades by large-domain, hecto-meter, large-eddy simulations. *Down to Earth*. <https://doi.org/10.31223/X5H651>
- Scott, R. C., Myers, T. A., Norris, J. R., Zelinka, M. D., Klein, S. A., Sun, M., & Doelling, D. R. (2020). Observed sensitivity of low-cloud radiative effects to meteorological perturbations over the global oceans. *Journal of Climate*, *33*(18), 7717–7734. <https://doi.org/10.1175/jcli-d-19-1028.1>
- Seifert, A., & Heus, T. (2013). Large-eddy simulation of organized precipitating trade wind cumulus clouds. *Atmospheric Chemistry and Physics*, *13*(11), 5631–5645. <https://doi.org/10.5194/acp-13-5631-2013>
- Sherwood, S. C., Webb, M. J., Annan, J. D., Armour, K. C., Forster, P. M., Hargreaves, J. C., et al. (2020). An assessment of Earth's climate sensitivity using multiple lines of evidence. *Reviews of Geophysics*, *58*(4), e2019RG000678. <https://doi.org/10.1029/2019rg000678>
- Stephens, G. L. (1978). Radiation profiles in extended water clouds. II: Parameterization schemes. *Journal of the Atmospheric Sciences*, *35*(11), 2123–2132. [https://doi.org/10.1175/1520-0469\(1978\)035<2123:rpiewc>2.0.co;2](https://doi.org/10.1175/1520-0469(1978)035<2123:rpiewc>2.0.co;2)
- Stevens, B., & Seifert, A. (2008). Understanding macrophysical outcomes of microphysical choices in simulations of shallow cumulus convection. *Journal of the Meteorological Society of Japan. Ser. II*, *86*, 143–162. <https://doi.org/10.2151/jmsj.86a.143>
- Tan, Z., Schneider, T., Teixeira, J., & Pressel, K. G. (2017). Large-eddy simulation of subtropical cloud-topped boundary layers: 2. Cloud response to climate change. *Journal of Advances in Modeling Earth Systems*, *9*(1), 19–38. <https://doi.org/10.1002/2016ms000804>
- Vial, J., Albright, A. L., Vogel, R., Musat, I., & Bony, S. (2023). Cloud transition across the daily cycle illuminates model responses of trade cumuli to warming. *Proceedings of the National Academy of Sciences*, *120*(8), e2209805120. <https://doi.org/10.1073/pnas.2209805120>
- Vial, J., Dufresne, J.-L., & Bony, S. (2013). On the interpretation of inter-model spread in CMIP5 climate sensitivity estimates. *Climate Dynamics*, *41*(11–12), 3339–3362. <https://doi.org/10.1007/s00382-013-1725-9>
- Vial, J., Vogel, R., & Schulz, H. (2021). On the daily cycle of mesoscale cloud organization in the winter trades. *Quarterly Journal of the Royal Meteorological Society*, *147*(738), 2850–2873. <https://doi.org/10.1002/qj.4103>
- Vogel, R., Albright, A. L., Vial, J., George, G., Stevens, B., & Bony, S. (2022). Strong cloud–circulation coupling explains weak trade cumulus feedback. *Nature*, *612*(7941), 696–700. <https://doi.org/10.1038/s41586-022-05364-y>
- Vogel, R., Nuijens, L., & Stevens, B. (2016). The role of precipitation and spatial organization in the response of trade-wind clouds to warming. *Journal of Advances in Modeling Earth Systems*, *8*(2), 843–862. <https://doi.org/10.1002/2015ms000568>
- Vogel, R., Nuijens, L., & Stevens, B. (2019). Influence of deepening and mesoscale organization of shallow convection on stratiform cloudiness in the downstream trades. *Quarterly Journal of the Royal Meteorological Society*, *146*(726), 174–185. <https://doi.org/10.1002/qj.3664>
- Wood, R., & Bretherton, C. S. (2006). On the relationship between stratiform low cloud cover and lower-tropospheric stability. *Journal of Climate*, *19*(24), 6425–6432. <https://doi.org/10.1175/jcli3988.1>
- Wood, R., O. K.-T., Bretherton, C. S., Mohrmann, J., Albrecht, B. A., Zuidema, P., et al. (2018). Ultraclean layers and optically thin clouds in the stratocumulus-to-cumulus transition. Part I: Observations. *Journal of the Atmospheric Sciences*, *75*(5), 1631–1652. <https://doi.org/10.1175/jas-d-17-0213.1>
- Zelinka, M. D., Myers, T. A., McCoy, D. T., Po-Chedley, S., Caldwell, P. M., Ceppi, P., et al. (2020). Causes of higher climate sensitivity in CMIP6 models. *Geophysical Research Letters*, *47*(1), e2019GL085782. <https://doi.org/10.1029/2019gl085782>
- Zhao, G., & Di Girolamo, L. (2007). Statistics on the macrophysical properties of trade wind cumuli over the tropical western Atlantic. *Journal of Geophysical Research*, *112*(D10). <https://doi.org/10.1029/2006jd007371>